Journal of Science and Technology in Civil Engineering, HUCE, 2025, 19 (2): 32–47

AN ANALYTICAL MODEL FOR EVALUATING LATERAL LOAD-DISPLACEMENT CURVE OF CORRODED REINFORCED CONCRETE BEAMS UNDER CYCLIC LOADING

Dang-Nguyen Nguyen[a,*]

[a]*Faculty of Building and Industrial Construction, Hanoi University of Civil Engineering, 55 Giai Phong road, Hai Ba Trung district, Hanoi, Vietnam*

Article history:
Received 10/4/2025, Revised 25/5/2025, Accepted 03/6/2025

Abstract

This paper presents an analytical model for evaluating the nonlinear response of corrosion-affected reinforced concrete (RC) beams under cyclic loading conditions. The analytical model addresses the interdependent flexural and shear mechanisms through two key components: (i) a flexural analysis module employing moment-curvature relationships that integrate corrosion-induced material deterioration in the concrete cover, tension in longitudinal reinforcement, buckling effects of compressive longitudinal reinforcement, along with plastic hinge length reduction; and (ii) a modified shear capacity model based on Sezen and Moehle's model but incorporating ductility-related strength reduction and corrosion damage parameters for both concrete and transverse reinforcement. The model was validated against experimental data from cyclic loading tests on eleven corroded RC beams. The results indicate that the model can accurately predict the load-displacement curve and failure mode to a reasonable extent. A strong correlation with the experimental peak load was observed, with an average ratio of 1.03 and a coefficient of variation (COV) of 0.08. However, the predictions for ultimate displacement show more variability, with an average ratio of 0.94 and a COV of 0.32.

Keywords: reinforced concrete; corrosion; cyclic loading; shear strength, ductility.

https://doi.org/10.31814/stce.huce2025-19(2)-03 © 2025 Hanoi University of Civil Engineering (HUCE)

1. Introduction

Chloride-induced corrosion of reinforcing bars plays a crucial role in the degradation of RC structures, reducing their service life. As corrosion increases, the load-bearing capacity of the affected member diminishes over time, mainly due to the progressive loss of steel cross-sectional area, crack formation, eventual spalling of the concrete cover, and a weakened bond between the steel reinforcement and the concrete. The decrease in load-carrying capacity due to corrosion poses a significant threat to structural safety, making corrosion-related damage a critical concern [1–7].

Displacement-based seismic design for new RC structures and the seismic assessment of existing RC structures require a comprehensive understanding of the lateral load-displacement behavior of RC elements [8–10]. ATC-40 [8], FEMA 273 [9], and FEMA 356 [10] specify the minimum acceptable values for the plastic hinge characteristics of RC members, taking into account factors such as their role in the structural system, reinforcement details, material properties, applied loads, and geometric features. Consequently, there has been growing interest in recent years in estimating the load-displacement capacity of RC members [3, 5–7, 11, 12].

Numerous experimental studies [13–16] have demonstrated that plastic hinge regions of RC members under cyclic loading can experience premature shear failure following the yielding of longitudinal reinforcement. These investigations highlight that inelastic deformations substantially reduce

*Corresponding author. *E-mail address:* nguyennd@huce.edu.vn (Nguyen, D.-N.)

shear capacity, with degradation occurring more rapidly than flexural strength under cyclic loading. Modern design standards, including ACI 318-19 [17] and NZS-3101 [18], recognize this strength reduction but adopt a conservative approach without explicitly linking it to member deformation levels. Notably, ACI 318-19 [17] disregards concrete's shear contribution in seismic design when axial compression is low, while NZS-3101 [18] entirely neglects concrete's role in shear resistance for such members.

Studies [1–3] have shown that transverse reinforcement corrodes faster than longitudinal bars owing to its smaller cross-section and reduced concrete cover, leading to more severe volumetric loss. This accelerated deterioration causes a shift in failure behavior-beams originally designed for ductile flexural failure increasingly exhibit flexural-shear or shear-dominated failure modes as corrosion increases. Consequently, the structural response becomes more brittle, significantly affecting the lateral force-displacement characteristics by intensifying shear influences.

Previous research on modeling the lateral force-displacement response of corroded RC members has primarily employed finite element analysis techniques [6, 7]. Among alternative approaches, Ou and Nguyen [3] developed the Modified axial-shear-flexure Interaction (MASFI) methodology and its corrosion-adapted version (MASFI-C), implementing these models through MATLAB-based computational procedures. While accurate, such numerical methods are quite complicated and demand significant computational resources [2, 5, 6]. Sectional analysis approaches based on the plane-sections-remain-plane assumption have also been proposed [11, 12], though these methods present limitations. Specifically, they fail to consider scenarios where shear capacity may exceed flexural strength and omit the progressive degradation of shear resistance with increasing ductility demands.

This study developed an analytical model for predicting the nonlinear load-displacement behavior of corrosion-damaged RC beams exhibiting significant shear strength deterioration post-yielding under cyclic loads. The proposed model integrates both flexural and shear mechanisms through a coupled analytical approach. For flexural response evaluation, moment-curvature analysis is employed incorporating corrosion-induced material degradation effects in cover concrete, tension in longitudinal reinforcement, buckling effect of compressive reinforcement, and plastic hinge length reduction. The shear capacity adapts the Sezen and Moehle [16] model by introducing: (i) a ductility-dependent reduction factor and (ii) corrosion-induced deterioration parameters accounting for both concrete strength loss and transverse reinforcement section reduction. Model validation is performed against experimental results from cyclic tests on eleven corroded RC beams.

2. Experimental data of corroded RC beams

This study uses experimental results from Ou and Chen [1] and Ou and Nguyen [2] to validate the analytical model. The beams used are labeled as TB, TBH, Bt, and B. Each experimental sample consists of a beam connected to a foundation block. The beam has a cross-sectional width (b_w) of 300 mm and a height (h) of 500 mm. The longitudinal reinforcement in both the upper and lower layers consists of three D29 bars. The shear reinforcement is provided by D13a100 bars spaced along the length of the beam. The actual material properties of the experimental beams can be found in the works of Ou and Chen [1] and Ou and Nguyen [2]. Apart from the control beam Bt-0, which is not corroded, the remaining beams were subjected to accelerated corrosion through an electrochemical corrosion process. The corrosion zone of the steel reinforcement is located in the plastic hinge region with a length of 600 mm from the bearing edge. Corrosion-induced cracks were measured on all four surfaces of the beam (top face, bottom face, and both side faces) within the 600 mm corrosion-affected zone. For each selected cross-section, the total crack width was obtained by summing the individual crack widths measured along the cross-section's perimeter. The 600 mm corroded length

was divided into six equal 100 mm segments along the beam's longitudinal axis, with crack width measurements taken for each segment. The average value of total crack widths (w_{cr}) presented in Table **??** corresponds to the average total crack width calculated across these six segments. Specimens of types Bt, TB, and TBH were intentionally subjected to corrosion in the transverse reinforcement, the top and bottom longitudinal reinforcement, and all reinforcement, respectively, within a 600 mm corroded region. The reinforcement located within and adjacent to the intended corroded area, but not meant to be affected by corrosion, was coated with a corrosion-inhibiting layer to prevent the spread of corrosion. However, experimental results showed that in the TB specimens, corrosion still occurred in the stirrups despite the application of epoxy coating, as can be seen in Table 1. The number at the end of each specimen name indicates the average actual corrosion weight loss. For specimen types TB and TBH, it represents the average weight loss of all longitudinal reinforcement within the corroded region [2]. For specimen type Bt, it corresponds to the average weight loss of all transverse reinforcement in the corroded region [1]. The value Δw is determined by dividing the difference in weight before and after corrosion by the original weight, assuming uniform corrosion along the length of the steel bar. The value $A_{st,\text{avg}}$ is calculated based on $\Delta w$of transverse reinforcement, while $\Delta w_{\max}$ is derived from $A_{st,\min}$. $A_{st,\min}$ represents the minimum residual cross-sectional area along the corroded transverse reinforcement. The corrosion levels at each steel reinforcement location, along with the methodology for determining the average value of total crack widths (w_{cr}), are provided elsewhere in [1-2]. Table 1 presents the material properties, steel reinforcement corrosion levels, and average value of total crack widths of the experimental beams. The beams were subjected to cyclic loading applied at a distance of 1200 mm from the bearing edge. Fig. 1 illustrates the design of the experimental beam.

Table 1. Material properties, reinforcement corrosion and crack width [1, 2]

Beam	f_c'	f_{yt}	f_{sYx}/f_{sux}	Longitudinal reinforcement	Transverse reinforcement				Crack width
				Δw (%)	Δw (%)	$\Delta w_{\max}$ (%)	$A_{st,\text{avg}}$ (mm^2)	$A_{st,\min}$ (mm^2)	w_{cr} (mm)
Bt-0	38	432	444/650	0.00	0.00	0.00	126.67	126.67	0.00
Bt-3				0.00	2.90	21.96	123.00	98.85	0.27
Bt-6				0.00	5.87	33.76	119.23	83.91	0.65
Bt-11				0.00	11.73	44.38	111.81	70.45	1.38
Bt-12				0.00	12.40	38.44	110.96	77.98	1.70
Bt-16				0.00	15.67	53.19	106.82	59.29	1.93
Bt-35				0.00	35.06	100.00	82.26	0.00	4.06
TBH-4	30	440	460/658	4.11	15.74	68.32	106.73	40.13	1.66
TBH-6				5.50	16.43	46.86	105.86	67.32	2.66
TB-6				6.51	6.54	31.81	118.39	86.37	2.30
TB-13				13.43	10.90	35.60	112.86	81.57	2.83

Note: f_c' is actual concrete compressive strength (MPa); f_{yt} is actual yield strength of uncorroded transverse reinforcement (MPa); f_{sYx} is actual yield strength of uncorroded longitudinal reinforcement (MPa); Δw = average corrosion weight loss; $A_{st,\text{avg}}$ is average residual cross-sectional area of transverse reinforcement, $A_{st,avg} = \left(\pi D_{0,t}^2/4\right)(1 - 0.01 \times \Delta w)$; $A_{st,\min}$ is minimum residual cross-sectional area of transverse reinforcement; $\Delta w_{\max}$ is maximum corrosion weight loss of transverse reinforcement, $\Delta w_{\max} = \left(1 - 4A_{st,\min}/\pi D_{0,t}^2\right)100$; $D_{0,t}$ is uncorroded diameter of transverse reinforcement; and w_{cr} is average value of total crack widths.

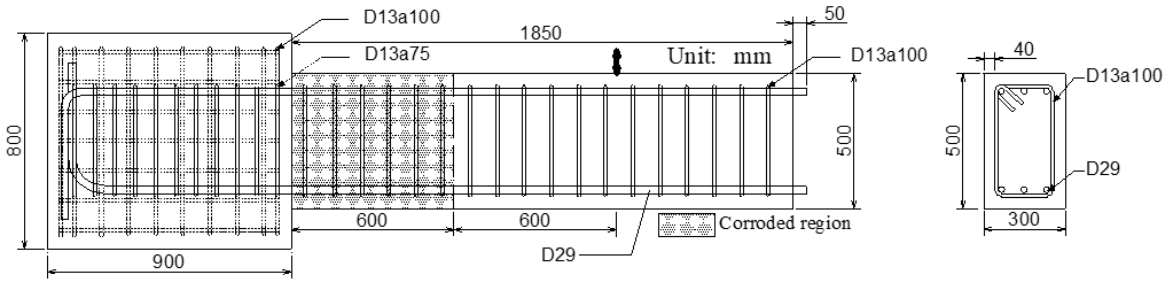

Figure 1. Experimental specimen [1, 2]

3. Analytical model for predicting combined flexure and shear behavior in corroded RC beams

3.1. Material models

a. Steel reinforcement in tension

The tensile stress-strain relationship of steel was modeled based on Mander's approach [19]. To enhance the accuracy of slip response predictions, a post-yield slope ($E'_s = 0.02E_s$) was incorporated into the yield plateau, accounting for strain hardening effects as recommended by Sezen and Setzler [20].

$$f_s = \begin{cases} E_s\varepsilon_s & \text{for } \varepsilon_s \le \varepsilon_{sY} \\ f_{sY} + 0.02E_s(\varepsilon_s - \varepsilon_{sY}) & \text{for } \varepsilon_{sY} \le \varepsilon_s \le \varepsilon_{sh} \\ f_{su} + (f_{sh} - f_{su})\left(\dfrac{\varepsilon_{su} - \varepsilon_s}{\varepsilon_{su} - \varepsilon_{sh}}\right)^2 & \text{for } \varepsilon_{sh} \le \varepsilon_s \le \varepsilon_{su} \end{cases} \quad (1)$$

where f_s is strength of the tensile steel at the strain ε_s; ε_s is strain of the tensile steel; ε_{sY} is yield strain of the tensile steel; ε_{sh} is strain at starting point of hardening; ε_{su} is ultimate strain of the tensile steel; f_{sY} is yield strength of the tensile steel; f_{sh} is strength of the tensile steel at starting point of hardening ($f_{sh} = f_{sY}+0.02E_s(\varepsilon_{sh} - \varepsilon_{sY})$); f_{su} is ultimate strength of the tensile steel; E_s is Young's modulus of steel in elasticity.

The loss of reinforcement cross-sectional area due to corrosion is modeled by Eq. (2), assuming a uniform distribution along the bar length. However, experimental studies show that yield and ultimate strengths are more strongly influenced by the minimum remaining cross-section rather than the average reduction accounted for in Eq. (12). Thus, these strength values are adjusted using Eq. (3) [21]. Given that corrosion minimally impacts the ultimate-to-yield strength ratio, hardening strain, and elastic modulus [22], these properties are maintained at their original (uncorroded) values.

$$A_s(\Delta w) = \frac{\pi D_0^2}{4}(1 - 0.01 \times \Delta w) \quad (2)$$

where $A_s(\Delta w)$ is cross-sectional area of a corroded bar depending on corrosion level (Δw); Δw is average corrosion weight loss (%); and D_0 is uncorroded bar diameter.

$$f_s^C = (1 - \beta\Delta w)\, f_0 \quad (3)$$

wheref_0 is uncorroded yield strength (f_{sY0}) or ultimate strength (f_{su0}); and f_s^C is corroded yield strength (f_{sY}^C) or ultimate (f_{su}^C) strength. In this work, $\beta = 0.005$ as recommended by Du et al. [21].

Stress concentrations near corrosion pits cause localized strain and stress amplification, triggering rebar fracture at average strains below the ultimate strain capacity of intact reinforcement [22–24]. The empirical formulation proposed by Du et al. [22] provides a means to estimate the residual

ultimate strain in corroded bars. Under seismic loading, longitudinal rebars in plastic hinge zones experience cyclic inelastic deformations, where premature failure occurs through two dominant modes: low-cycle fatigue and lateral buckling. Consequently, the strain capacity deteriorates markedly under cyclic loading relative to monotonic conditions. To account for this reduction, Yeh et al. [24] suggest employing a ductility reduction factor (ψ) between 0.6 and 0.7. In this analysis, ψ value of 0.7 is adopted in this study to determine ultimate strain limits.

$$\varepsilon_{su}^{C} = \psi\,(1 - \alpha\Delta w)\,\varepsilon_{su0} \tag{4}$$

where ε_{su}^{C} is ultimate strain of corroded reinforcement; ε_{su0} is ultimate strain of uncorroded steel; ψ is coefficient to consider the effect of low-cycle fatigue ($\psi = 0.7$); α = ultimate strain factor for longitudinal reinforcement. Through analysis of experimental results, Du et al. [22] established that the coefficient ranges from 0 to 0.06, with its value being dependent on corrosion severity. Their research led to the recommendation of for exposed reinforcement and for concrete-encased bars. For this investigation, a baseline value of 0.03 was initially employed in the preliminary evaluation. Further refinements were then implemented for cases where bar fracture occurred to establish optimal coefficient values. Fig. 2(a) presents an example of stress-strain relationships under tension for corroded and uncorroded steel reinforcement.

b. Steel reinforcement in compression

To characterize steel reinforcement under compression, the tensile stress-strain curve defined by Eq. (1) is adapted. Dhakal and Maekawa's [25] proposed modifications are applied to consider compressive buckling effects. Corrosion influences are addressed through calibration of the buckling parameter (λ_p^C) in Eq. (5), which governs the compressive yield strength (f_{sYc}^C), and residual bar diameter (D_c). The strength reduction factor (β_c) in Eq. (6) correlates with the slenderness ratio of corroded reinforcement [26].

$$\lambda_p^C = \sqrt{\frac{f_{sYc}^C}{100}}\frac{L_{bl}}{D_c} \tag{5}$$

$$f_{sYc}^C = f_{sY}\,(1 - \beta_c\Delta w) \tag{6}$$

where λ_p^C is non-dimension bar buckling parameter of corroded bars; f_{sYc}^C is yield stress of corroded steel under compression (in MPa); D_c is corroded bar diameter determined according to average weight loss = $D_0\sqrt{1 - 0.01\Delta w}$; β_c is empirical factor ($\beta_c = 0.005$ for $L_{bl}/D_c \le 5$, $\beta_c = 0.0065$ for $L_{bl}/D_c \le 10$, and $\beta_c = 0.0125$ for $L_{bl}/D_c > 10$); and L_{bl} is buckling length.

Given non-dimensional stress $\eta = f_{sc}/f_{sYc}^C$ and strain $\xi = \varepsilon_{sc}/\varepsilon_{sYc}^C$ (where $\varepsilon_{sYc}^C = f_{sYc}^C/E_s$) the buckling model for steel reinforcement in compression conforming to Kashani et al [26] is given as follows:

$$\eta = \begin{cases} \xi & \text{for } \xi \le 1 \\ \dfrac{\eta_2 - 1}{\xi_2 - 1}(\xi - 1) + 1 & \text{for } 1 < \xi \le \xi_2 \\ \eta_2 - 0.02(\xi - \xi_2) & \text{for } \xi_2 \le \xi \text{ and } \eta \ge 0.2 \\ 0.2 & \text{otherwise} \end{cases} \tag{7}$$

where the empirical relationships for (η_2, ξ_2) are given below:

$$\xi_2 = 55 - 2.3\lambda_p^C \text{ for } \xi \ge 7 \tag{8}$$

$$\eta_2 = \alpha\left(1.1 - 0.016\lambda_p^C\right)\eta_2^* \text{ for } \eta_2 \geq 0.2 \tag{9}$$

where η_2^* is the non-dimensional piecewise stress corresponding to the ξ_2. The value of α is a softening coefficient and depends on the strain hardening of reinforcement. The following equations are recommended to compute α [25]:

$$\alpha = 0.75 + \frac{\varepsilon_{su} - \varepsilon_{sh}}{300\varepsilon_{sY}}; \quad \alpha \leq \frac{f_{su}}{1.5f_{sY}}; \quad 0.75 \leq \alpha \leq 1 \tag{10}$$

Transverse reinforcement in RC structures performs three primary functions: (i) resisting shear forces, (ii) confining the concrete core, and (iii) preventing buckling of longitudinal reinforcement. Each of these roles generates distinct stress and strain distributions in the transverse reinforcement. Shear resistance typically dominates during initial loading stages, preceding the activation of confinement and buckling resistance. As a result, the concurrent presence of shear reduces the transverse reinforcement's capacity to mitigate confinement loss and restrain buckling. Ou and Nguyen [3] analytically delineated the interplay between shear, confinement, and buckling effects on transverse reinforcement behavior. In this study, the transverse reinforcement is assumed to contribute solely to shear resistance, with no consideration for its role in confinement or buckling restraint. Consequently, the buckling length (L_{bl}), defined as the unsupported length of longitudinal bars prone to instability, is taken as equal to the plastic hinge length, which is assumed to match the section depth (h). This simplification is justified by the localization of buckling within the plastic hinge region, where severe concrete cover spalling and inelastic deformations concentrate. For cyclically loaded flexural members, empirical and analytical evidence supports the adoption of h as a representative plastic hinge length (Scribner [27]). Fig. 2(b) illustrates an example of stress-strain relationships under compression for corroded and uncorroded steel reinforcement.

c. Concrete

The compressive behavior of cover and core concrete is simulated using the unconfined concrete model developed by Mander et al. [28]. Corrosion of steel reinforcement impacts only the cover concrete, not the inner concrete core. As a result, the mechanical properties of the core concrete are not affected by tensile stresses from the volume expansion of corrosion products and are treated as if the concrete were unaffected by corrosion. However, the compressive behavior of the cover concrete is degraded due to the formation of corrosion products. Corrosion-induced volumetric expansion generates tensile strain in the cover concrete (ε_r), which reduces its compressive strength. This strain is derived from the total crack width (w_{cr}) via Eq. (11), while the residual compressive strength of the cover concrete, $\xi f_c'$, due to corrosion is quantified using Eq. (12). The softening coefficient was proposed by Hsu [29].

$$\varepsilon_r = \frac{w_{cr}}{p_{cp}} = \frac{\sum w_{cr,i}}{p_{cp}} \tag{11}$$

$$\xi = \frac{0.9}{\sqrt{1 + 600\varepsilon_r}} \tag{12}$$

where ε_r is tensile strain induced to cover concrete; w_{cr} is total crack width over pcp; $w_{cr,i}$ is crack width of the ith corrosion crack; p_{cp} is the length along the cross-sectional perimeter over which the total crack width of corrosion cracks is calculated.

Fig. 2(c) shows the effect of corrosion on cover and core concrete. The tensile capacity of concrete is considered negligible in the analytical model.

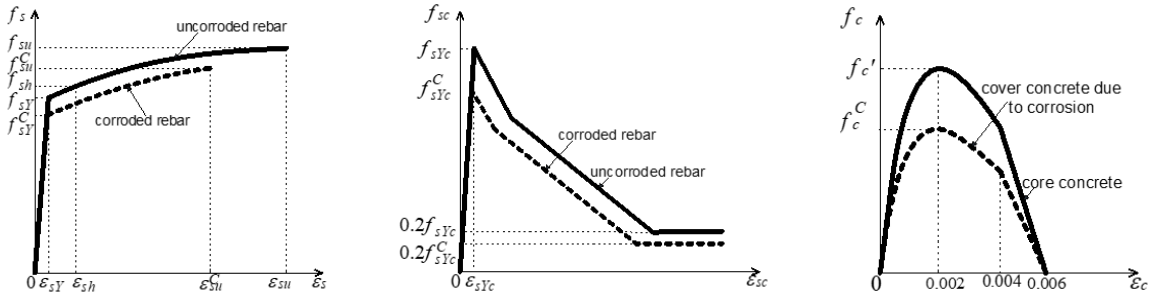

(a) Rebar in tension (b) Rebar in compression (c) Concrete in compression

Figure 2. Corroded and uncorroded material models

3.2. Flexure capacity

The drift ratio at the loading point (θ) of a RC beam can be expressed as follows:

$$\theta = \theta_{shear} + \theta_{flex} + \theta_{pull} \tag{13}$$

where θ is total drift, θ_{shear} is shear drift, θ_{flex} is drift due to flexure, and θ_{pull} is drift due to longitudinal reinforcement of the beam pull out from the anchorage block. For all test beams with a span-to-depth ratio (L/d) of 2.8, flexural deformation dominates and shear deformation is neglected [30].

Flexural drift θ_{flex} of the beam is determined as follows:

$$\theta_{flex} = \begin{cases} \dfrac{1}{3}\phi L & \text{for } \phi \le \phi_y \\ \dfrac{1}{3}\phi L + (\phi - \phi_y)(L - 0.5L_p)L_p & \text{for } \phi > \phi_y \end{cases} \tag{14}$$

where ϕ is the curvature of the cross-section determined from the moment-curvature analysis using Xtract software [31]; ϕ_y is the curvature of the cross-section corresponding to the time when the longitudinal reinforcement reaches yielding in tension; L is the length of the beam. In the moment-curvature analysis determined by Xtract software [31], the cross-section of the beam is divided into material fibers with properties defined according to the material models described in Section 3.1. The curvature (ϕ) is gradually increased from zero until the cross-section is considered to have failed, corresponding to either the crushing of the cover concrete or the rupture of the tension longitudinal reinforcement. It is also assumed that, once the cross-section fails, it entirely loses its load-carrying capacity, and the moment resistance of the section drops to zero immediately. There are several recommendations in the literature regarding the ultimate compression strains for cover concrete. The commonly used value is 0.003, as specified in ACI 318-19 [17]. This value is valid for concrete elements subjected to uniaxial compressive loading or constant moment. However, concrete elements under significant moment gradients can sustain strains of approximately 0.006 to 0.008 [32]. Mander et al. [28] proposed that cover concrete begins to spall when its compressive strain reaches 0.004 and fully spalls when the compressive strain reaches 0.006. In the moment-curvature analysis, the analysis will be terminated when one of the following two conditions occurs: either when the strain at the outermost compression fiber of the cover concrete reaches 0.004, or when the ultimate strain of the tensile reinforcement reaches the limit value calculated according to Eq. (4). The ultimate compressive strain value of 0.004 adopted in this study follows conventional assumptions for uncorroded concrete. Under significant corrosion conditions, this assumption may not accurately represent

the concrete's true strain capacity. Therefore, further experimental and analytical investigations are needed to examine corrosion-induced degradation of compressive strain capacity and thereby enhance modeling reliability. The moment (M_b) corresponding to the curvature (ϕ) is determined by calculating the moment of the material fibers in the cross-section with respect to the neutral axis. The shear demand value (V_b) is determined by dividing the moment value (M_b) by the span length (L).

The plastic hinge length (L_p) for uncorroded specimens was determined to be equal to the section depth (h), in line with the guidelines provided by Moehle [33], Setzler and Sezen [20], and Lodhi and Sezen [34]. It was assumed that corrosion in transverse reinforcement had minimal impact on L_p, while corrosion in longitudinal reinforcement resulted in a reduction of L_p. For corroded beams, the L_p was calculated based on the modification method suggested by Ou and Nguyen [35]. The L_p was observed to reduce to 98%, 96%, 88%, and 80% of the uncorroded value at corrosion levels of 10%, 15%, 20%, and 25%, respectively. For corrosion levels below 25%, L_p was estimated using linear interpolation, while for corrosion levels above 25%, L_p was assumed to be the same as the value at 25% corrosion.

The slip rotation (θ_{pull}) was calculated using the Sezen and Setzler model [20] as presented in Fig. 3.

$$\theta_{pull} = \begin{cases} \dfrac{\varepsilon_{sx} f_{sx} d_b}{8 u_b (d-c)} & \text{for } \varepsilon_{sx} \le \varepsilon_{sYx} \\ \dfrac{d_b}{8 u_b (d-c)} \left(\varepsilon_{sYx} f_{sYx} + 2(\varepsilon_{sx} + \varepsilon_{sYx})(f_{sx} - f_{sYx})\right) & \text{for } \varepsilon_{sx} > \varepsilon_{sYx} \end{cases} \tag{15}$$

where ε_{sx} and f_{sx} are the strain and stress of the longitudinal reinforcement, respectively; ε_{sYx} and f_{sYx} are the yield strain and yield stress of the longitudinal reinforcement, respectively; d_b is the diameter of the longitudinal reinforcement; u_b is the uniform bond stress, taken as $\sqrt{f'_c}$ (f'_c in MPa); d is the distance from the extreme compression fiber to the centroid of the extreme layer of longitudinal tension reinforcement; and a is the neutral axis depth. The validation beams featured fully anchored longitudinal reinforcement. To isolate corrosion effects, synthetic rubber coatings were applied to the anchorage blocks, ensuring corrosion was confined to the exposed bar segments below the fixed-end interface. Consequently, the embedded regions maintained both corrosion-free conditions and pristine bond-slip characteristics equivalent to uncorroded reinforcement.

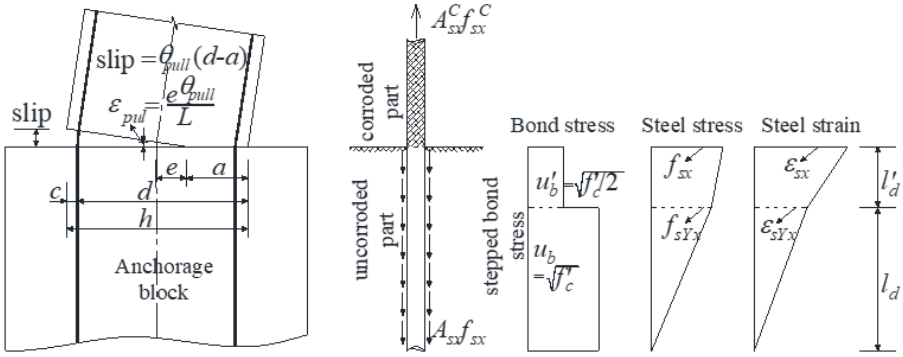

Figure 3. Pullout deformation model [20]

In Fig. 4(a), θ_y and θ_u represent the yield drift (corresponding to the point where the longitudinal reinforcement yields in tension) and the ultimate drift (corresponding to the point where the cover concrete crushes or the longitudinal reinforcement ruptures), respectively. $V_{b,y}$ and $V_{b,u}$ represent the flexure capacities of the beam corresponding to θ_y and θ_u, respectively.

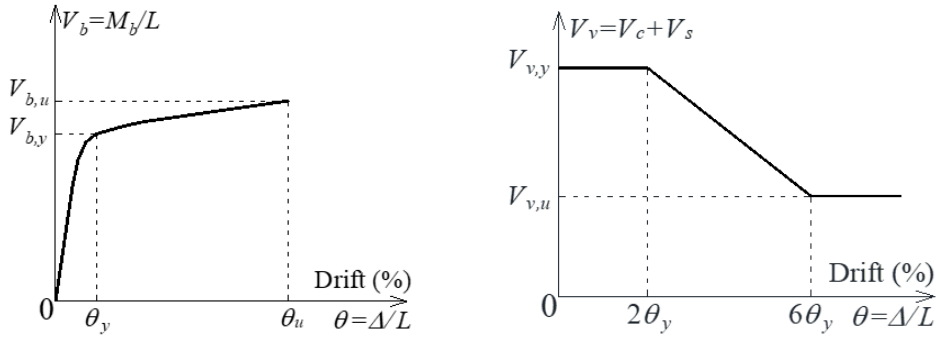

(a) Flexural capacity (b) Shear capacity

Figure 4. Flexural capacity and shear capacity of corroded RC beams

3.3. Shear capacity

During seismic events, the plastic hinge areas of a RC beam are anticipated to experience inelastic deformation cycles. It is well-established that the shear strength diminishes under such inelastic reversals as ductility increases. Sezen and Moehle [16] proposed a model to estimate the shear capacity of uncorroded lightly RC columns, incorporating the reduction in apparent strength due to flexural yielding. This study simply modified Sezen and Moehle [16] model to account for the effects of corrosion, while neglecting compressive axial load, in order to evaluate the shear capacity of corroded RC beams under cyclic loading. The shear strength of a corroded or uncorroded RC beam consists of two components: the shear strength contributed by the concrete (V_c) and the shear strength contributed by the shear reinforcement (V_s).

$$V_v = V_c + V_s \tag{16}$$

The models address the impact of corrosion by replacing the parameter f_c' with $\xi f_c'$ to account for the degradation of the cover concrete. Meanwhile, the compressive strength of the core concrete, denoted as f_c', remains unchanged. The contribution of the concrete will be calculated using Eq. (17):

$$V_c = V_{\text{c,cover}} + V_{\text{c,core}} = k\left(\frac{1}{L/d}\right)\left(0.5\sqrt{f_c'} \times A_{\text{core}} + 0.5\sqrt{\xi f_c'} \times A_{\text{cover}}\right) \tag{17}$$

where $V_{\text{c,cover}}$ is shear strength of cover concrete; $V_{\text{c,core}}$ is shear strength of core concrete; A_{core} is area of core concrete; A_{cover} is area of cover concrete; f_c' is compressive strength of concrete; L is distance from maximum moment section to point of inflection; the value of L/d is limited to $2 \leq L/d \leq 4$; $k = 1$ for $\mu \leq 2$, $k = 0.7$ for $\mu \geq 6$, with linear variation between these limits; $\mu = \Delta_u/\Delta_y$ = displacement ductility; Δ_u is ultimate displacement; Δ_y is yield displacement.

Corrosion-induced deterioration in RC beams leads to diminished shear capacity in transverse reinforcement, primarily through two mechanisms: reduced cross-sectional area and degraded material strength. For analytical modeling, shear-resisting ties are represented using a dual-area approach—one half characterized by the average residual area ($A_{st,\text{avg}}$) and the other by the minimum residual area ($A_{st,\text{min}}$). This methodology, experimentally validated by Ou and Chen [1], demonstrates improved accuracy in shear strength estimation. Notably, research findings [23] indicate that when strength calculations are based on $A_{st,\text{min}}$, corrosion has minimal effect on both yield and ultimate strength properties. Therefore, the original yield strength values are maintained for $A_{st,\text{min}}$-based calculations, while the corroded tensile strength from Eq. (6) is applied for $A_{st,\text{avg}}$ cases. The total shear reinforcement contribution is subsequently computed via Eq. (18).

$$V_s = k\frac{A_{st}^C f_{yt}^C d}{s} = k\frac{(A_{st,\text{avg}} f_{yt}^C + A_{st,\text{min}} f_{yt})d}{s} \tag{18}$$

where V_s is shear strength of transverse reinforcement due to corrosion; A_{st}^C is remaining area of corroded transverse reinforcement; f_{yt}^C is yield strength of corroded transverse reinforcement; $A_{st,\text{avg}}$ is average area of corroded transverse reinforcement; $A_{st,\text{min}}$ is minimum area of corroded transverse reinforcement; A_{core} is area of core concrete; A_{cover} is area of cover concrete; f_{yt} is yield strength of transverse reinforcement; d is effective section depth; s is spacing of transverse reinforcement.

The shear capacity of a corroded RC beam can be determined through the relationship between shear capacity (V_v) and total drift (θ), as illustrated in Fig. 4(b). In Fig. 4(b), $V_{v,y}$ (which remains constant for drifts from 0 to $2\theta_y$) and $V_{v,u}$ (which remains constant for drifts greater than $6\theta_y$) represent the shear capacities of the beam corresponding to the shear strength reduction factors due to increasing drift, with $k = 1$ and $k = 0.7$ in Eqs. (17) and (18), respectively. The above value of k, which represents the degradation of post-yield shear capacity, is determined based on the study by Sezen and Moehle [16].

Figs. 5(a), (b), and (c) respectively illustrate the contributions of the cover concrete, core concrete, and shear reinforcement to the shear strength of the corroded RC beam, which will be used for the shear capacity calculations.

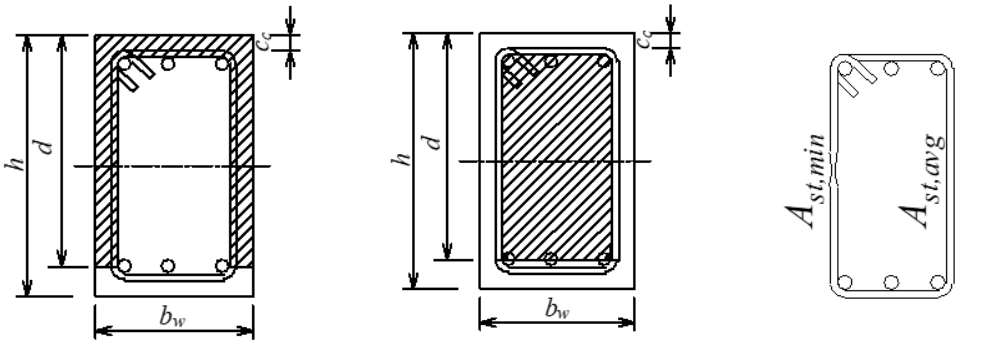

(a) Cover concrete (b) Core concrete (c) Shear reinforcement

Figure 5. Shear strength contribution

3.4. Interaction between flexure and shear capacity

The shear capacity (V_v, θ) is overlaid on the flexural capacity (V_b, θ) plot to examine combined response and the possible failure modes. This approach allows for the classification of three distinct failure modes, which are shear failure, flexure-shear failure, and flexure failure of corroded RC beams, as shown in Fig. 6(a), (b), and (c). The classification of failure modes (shear, flexure-shear, flexure) not only clarifies structural behavior but also aids practical assessment. A shift from flexural to shear-dominated failure often indicates reduced ductility and increased brittleness, which may require different strengthening or retrofitting approaches. Recognizing these modes can thus support more informed decisions in the maintenance and safety evaluation of corroded RC structures.

The $(V - \theta)$ diagram for the shear failure mode of corroded RC beams is depicted in Fig. 6(a). It is evident that $V_v < V_b$ in the inelastic region, which suggests that the shear strength is lower than the flexural strength, resulting in shear failure occurring before flexural failure. The $(V - \theta)$ diagram's features are outlined starting from point 0, passing sequentially through points A, B, and C, and

ending at point D in Fig. 6(a). Point 0 represents the origin. Point A marks the intersection of V_v and V_b, where $V_v = V_{v,y}$, and the corresponding coordinates are $(V_{v,y}, \theta_i)$, with θ_i determined by setting $V_b = V_{v,y}$. Finally, points "C" and "D" coincide at the coordinates $(V_{v,u}, 6\theta_y)$ and $(0, 6\theta_y)$, respectively. The combined response, labeled as "0$ABCD$" in Fig. 6(a), can be considered the load-displacement curve of corroded RC beams that failed in shear.

The flexure-shear failure mode diagram of corroded RC beams is shown in Fig. 6(b). Here, point "A" corresponds to the yielding of the longitudinal reinforcement. In this failure mode, the critical point "B" is located where V_v equals V_b, marking the transition from flexure to shear failure. The coordinates of point "B", denoted as (V_i, θ_i), can be obtained by solving the combined equations of the two failure mechanisms. It is clear that flexural failure governs the rotation range from 0 to θ_i, while shear failure dominates the subsequent range from θ_i to $6\theta_y$. Points "C" and "D" represent the final points, with coordinates $(V_{v,u}, 6\theta_y)$ and $(0, 6\theta_y)$, respectively. The combined response, labeled as "0$ABCD$" in Fig. 6(b), can be considered the load-displacement curve of corroded RC beams that failed in flexure-shear.

Fig. 6(c) depicts the flexure failure mode of corroded RC beams. It is evident that V_v remains consistently greater than V_b without any intersection, suggesting that flexural failure dominates the overall behavior of the corroded RC beams. Point "A" represents the yielding of the longitudinal reinforcement. Point "$B \equiv C$" indicates the critical point corresponding to either the crushing of the cover concrete or the rupture of the tension longitudinal reinforcement, as presented in Section 3.2, with coordinates $(V_{b,u}, \theta_u)$. The combined response, labeled as "0$ABCD$" in Fig. 6(c), can be considered the load-displacement curve of corroded RC beams that failed in flexure. In this case of failure, the combined response curve coincides with the flexural capacity curve.

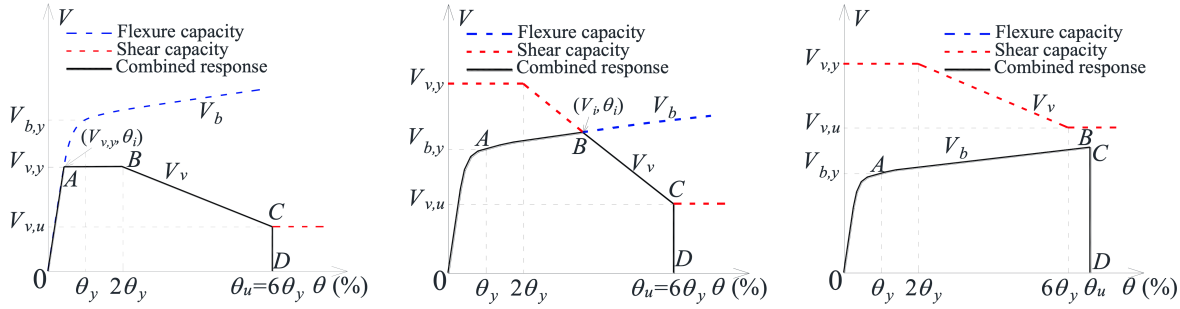

(a) Shear failure (b) Flexure-Shear failure (c) Flexure failure

Figure 6. Interaction of flexural and shear capacity of RC beams

4. Model validation

The experimental results of the beams summarized in Section 2 are used for comparison with the proposed computational model. Fig. 7 illustrates the comparison of the load-displacement curves between the experimental results and the proposed model for corroded RC beams, with corrosion occurring in the transverse reinforcement. Generally, the initial stiffness and strength show good consistency between the analytical and experimental results. The Bt-0 and Bt-3 beams are predicted to fail due to flexure, which is consistent with the experimental behavior observed for these beams, where the compressive strain at the outermost concrete fiber reaches 0.004. Therefore, in Figs. 7(a) and (b), the flexure capacity curve coincides with the combined response curve from the analysis. The Bt-6 beam is forecasted to fail due to flexure-shear at a drift level of 2.68%, where the flexure capacity curve intersects with the shear capacity curve as shown in Fig. 7(c). This predicted failure

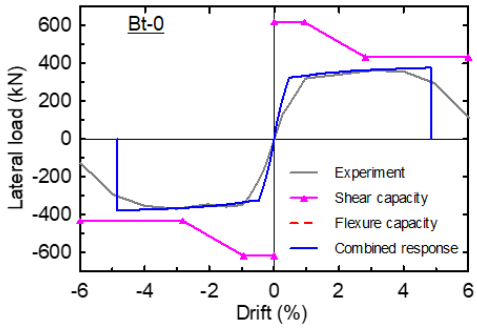

(a) Bt-0

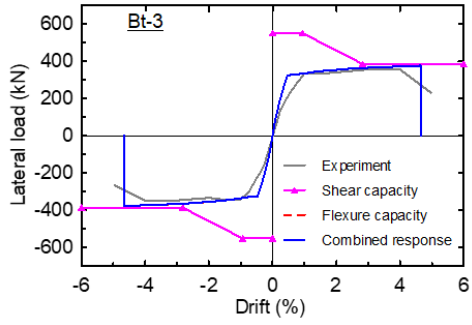

(b) Bt-3

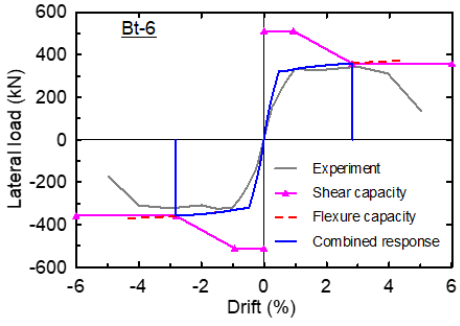

(c) Bt-6

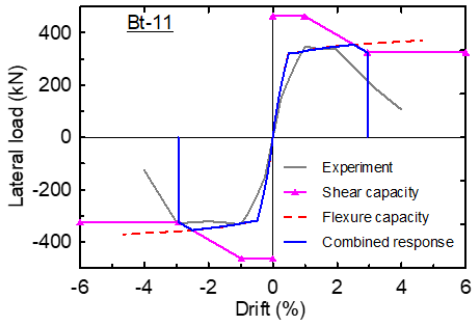

(d) Bt-11

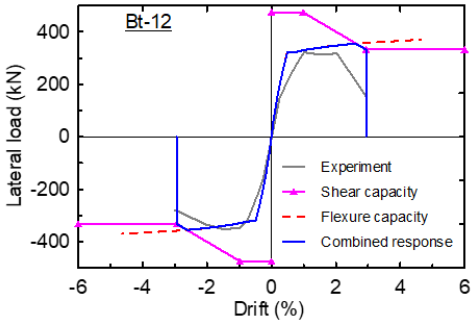

(e) Bt-12

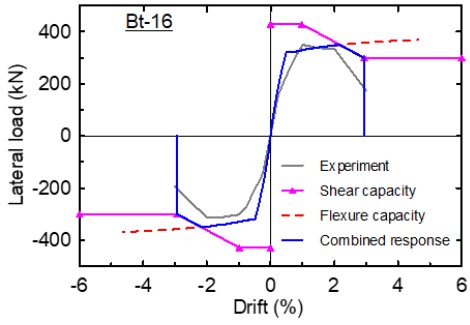

(f) Bt-16

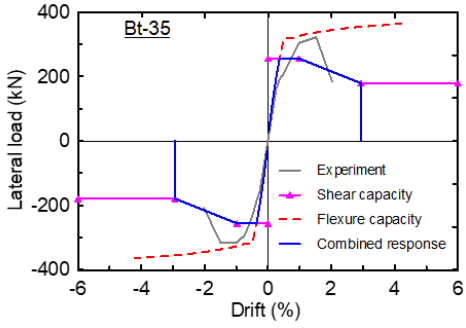

(g) Bt-35

Figure 7. Experimental and analytical result for Bt-type beams

mode matches the flexure-shear failure mode observed experimentally. However, in the experimental results, the beam failed in shear because the transverse reinforcement ruptured at a drift level of 4%. The Bt-11, Bt-12, and Bt-16 beams, as presented in Figs. 7(d), (e), and (f), show a strong agreement with experimental results in terms of stiffness and load-carrying capacity. These beams are predicted to fail due to flexure-shear, with longitudinal reinforcement yielding and corroded transverse reinforcement rupturing, which is consistent with experimental observations. It can be noted that the proposed model (represented by the combined curve) predicts the shear failure point at a higher drift displacement compared to the experimental results. The Bt-35 beam, which has corroded transverse reinforcement resulting in rupture, is predicted to fail in shear prior to the yielding of the longitudinal reinforcement as illustrated in Fig. 7(g). However, experimental observations indicate that the beam can tolerate flexure deformation up to a 2% drift, with the longitudinal reinforcement having already yielded, before shear failure occurs, as evidenced by the rupture of some transverse reinforcement.

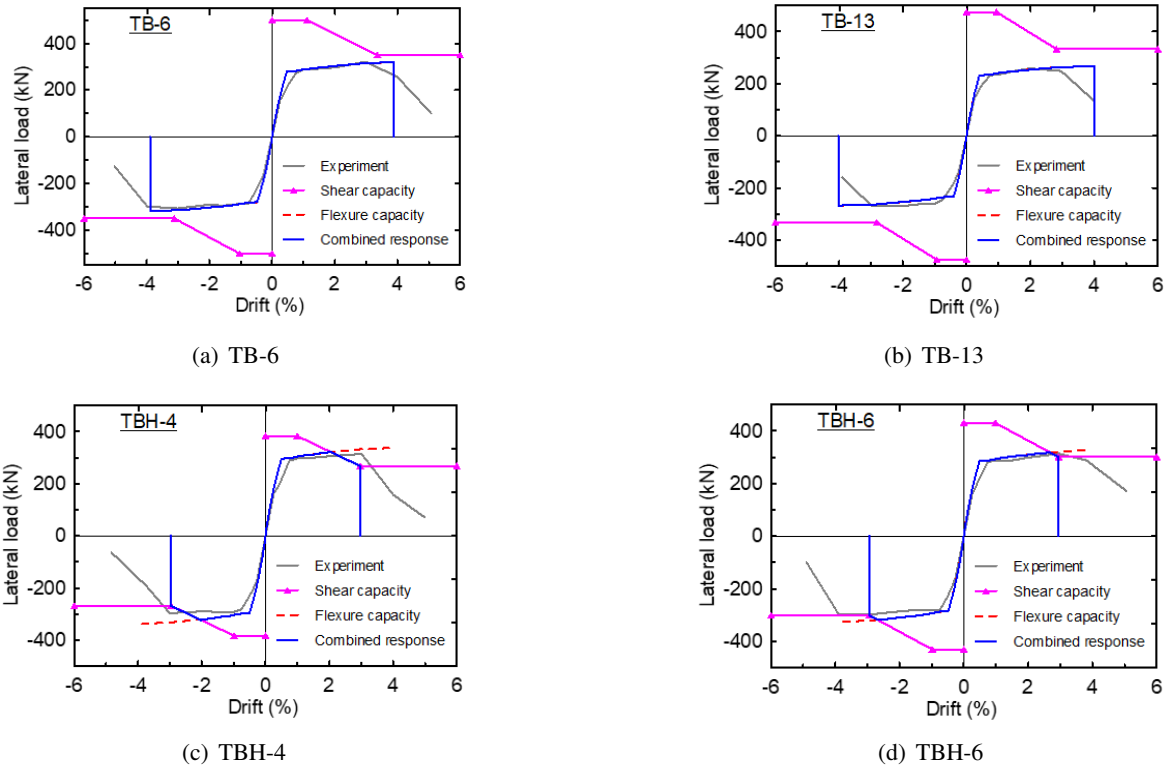

(a) TB-6 (b) TB-13

(c) TBH-4 (d) TBH-6

Figure 8. Experimental and analytical result for TB-, and TBH-type beams

Fig. 8 shows a comparison of the load-displacement curves between the experimental results and the proposed model for corroded RC beams, with corrosion induced both the longitudinal and transverse reinforcement. The analytical model accurately captured the initial stiffness, strength, and post-peak behavior of TB-6, TB-13, TBH-4, and TBH-6. The model predicted that the failure of the TB-6 and TB-8 specimens occurred due to flexure, with cover concrete crushing at a strain of 0.004 after the yielding of the corroded longitudinal reinforcement, which is consistent with the experimental observations. As a result, in Figs. 8(a) and (b), the flexure capacity curve aligns with the combined response curve obtained from the analysis. Good predictions of stiffness, strength, and failure mode are captured for specimen TBH-4 and TBH-6 as shown in Figs. 8(c) and (d), respectively. The analytical results and experiments showed that TBH-4 and TBH-6 failed in flexure-shear due to

the fracture of the corroded transverse reinforcement, similar to the failure mode observed in most Bt-type beams.

Table 2 summarizes the comparison between the experimental results and those obtained from the analytical model. The experimental performance indicators include the idealized yield force (P_y^{Exp}), yield drift (θ_y^{Exp}), peak force (P_p^{Exp}), and ultimate drift (θ_u^{Exp}). The peak force (P_p^{Exp}) represents the maximum applied load recorded during testing. The ultimate drift (θ_u^{Exp}) is defined as the drift corresponding to a 20% reduction in load from the peak value (P_p^{Exp}) along the envelope response. To identify this value, the envelope response is idealized using a bilinear relationship, as described in detail by Ou and Nguyen [2]. The θ_y^{Exp} is determined as the rotation at the intersection point of bilinear segments, and the corresponding load is defined as the yield load (P_y^{Exp}). Meanwhile, the P_y^{Pred} and θ_y^{Pred} represent yield load and yield drift obtained from the analytical model corresponding to yielding of longitudinal reinforcement. The P_p^{Pred} and θ_u^{Pred} are the ultimate load (corresponding to point B in Fig. 6) and ultimate drift (corresponding to point B in Fig. 6) predicted by the analytical model. The comparison between the analytical model and experimental results shows a strong correlation in terms of peak load, with an average ratio of 1.03 and a COV of 0.08. In contrast, the comparison of ultimate displacements between the analytical model and experimental data exhibits greater variability, with an average ratio of 0.94 and a COV of 0.32. As can be seen from Figs. 7 and 8, further investigation is recommended to enhance the analytical model's capability in predicting post-peak strength degradation.

Table 2. Comparison between experiment and analytical model

Beam	P_y^{Exp} (kN)	θ_y^{Exp} (%)	P_p^{Exp} (kN)	θ_u^{Exp} (%)	Exp./Pred. fail. mode	P_y^{Pred} (kN)	θ_y^{Pred} (%)	P_p^{Pred} (kN)	θ_u^{Pred} (%)	$\frac{P_p^{\text{Pred}}}{P_p^{\text{Exp}}}$	$\frac{\theta_u^{\text{Pred}}}{\theta_u^{\text{Exp}}}$
Bt-0	341.5	0.80	365.4	4.97	F/F	326.1	0.47	378.2	4.85	1.04	0.98
Bt-3	333.5	0.70	354.6	4.67	F/F	326.1	0.47	376.7	4.66	1.06	1.00
Bt-6	315.0	0.70	333.4	4.27	F-S/F-S	322.5	0.48	358.6	2.88	1.08	0.66
Bt-11	317.5	0.70	340.5	2.87	F-S/F-S	321.3	0.49	355.5	2.94	1.04	1.02
Bt-12	316.0	0.68	336.9	2.67	F-S/F-S	321.3	0.49	355.2	2.94	1.05	1.10
Bt-16	315.0	0.70	331.7	2.44	F-S/F-S	320.8	0.49	350.0	2.94	1.06	1.20
Bt-35	310.5	0.65	318.8	1.79	F-S/S	N.A	N.A	255.9	2.94	0.80	1.64
TBH-4	284.5	0.51	300.0	3.42	F-S/F-S	295.9	0.50	323.0	2.97	1.08	0.87
TBH-6	283.0	0.50	306.0	4.20	F-S/F-S	285.4	0.49	317.8	2.94	1.04	0.70
TB-6	292.0	0.54	314.0	4.15	F/F	280.3	0.47	320.0	3.89	1.02	0.94
TB-13	248.5	0.46	264.0	3.41	F/F	232.2	0.40	268.4	3.99	1.02	1.17
					Mean					1.03	0.94
					Coefficient of variation					0.08	0.32

Note: F-S = Flexure-Shear failure mode; S = Shear failure mode; F = Flexure failure mode; Exp./Pred. fail. Mode = Experiment/Predicted failure mode; N.A = Not applicable.

5. Conclusions

This study presents an analytical model to predict the nonlinear load-displacement response of corrosion-damaged RC beams, particularly under cyclic loading where significant shear strength deterioration occurs post-yielding. The model combines flexural and shear mechanisms using a coupled analytical framework. Flexural behavior is assessed through moment-curvature analysis, considering

material degradation in cover concrete, longitudinal reinforcement, and reduced plastic hinge length due to corrosion. For shear capacity, an adapted version of the Sezen and Moehle'model is used, incorporating two key modifications: (i) a reduction factor dependent on ductility and (ii) corrosion-related deterioration parameters that account for weakened concrete, reduced the yield strength and area of transverse reinforcement. The results demonstrate that the model effectively predicts both the load-displacement curve and failure mode with reasonable accuracy. A strong correlation with the experimental peak load was found, with an average ratio of 1.03 and a COV of 0.08. However, the predictions for ultimate displacement exhibit greater variability, showing an average ratio of 0.94 and a COV of 0.32.

Acknowledgements

The author would like to express sincere gratitude to Professor Dr. Yu-Chen Ou, of the Department of Civil Engineering at National Taiwan University (NTU), General Director of the National Center for Research on Earthquake Engineering (NCREE), Taiwan, for his invaluable guidance and support in the preparation of this paper.

References

[1] Ou, Y.-C., Chen, H.-H. (2014). Cyclic behavior of reinforced concrete beams with corroded transverse steel reinforcement. *Journal of Structural Engineering*, 140(9):04014050.

[2] Ou, Y.-C., Nguyen, N. D. (2016). Influences of location of reinforcement corrosion on seismic performance of corroded reinforced concrete beams. *Engineering Structures*, 126:210–223.

[3] Ou, Y.-C., Nguyen, N. D. (2016). Modified axial-shear-flexure interaction approaches for uncorroded and corroded reinforced concrete beams. *Engineering Structures*, 128:44–54.

[4] Nguyen, N. D., Tan, N. N. (2019). Prediction of residual carrying capacity of RC column subjected in-plane axial load considering corroded longitudinal reinforcement. *Journal of Science and Technology in Civil Engineering (SCTE) - NUCE*, 13(2V):53–62. (in Vietnamese).

[5] Nguyen, N. D., Hai, D. V. (2019). Prediction of lateral force-displacement response of simple span corroded reinforced concrete beams subjected to four-point bending. *Journal of Science and Technology in Civil Engineering (SCTE) - NUCE*, 13(4V):82–93. (in Vietnamese).

[6] Vu, N. S., Yu, B., Li, B. (2016). Prediction of strength and drift capacity of corroded reinforced concrete columns. *Construction and Building Materials*, 115:304–318.

[7] Nguyen, N. D., Tan, N. N., Thu, N. M. (2024). Investigation of factors affecting the load-carrying capacity of corroded circular reinforced concrete columns using finite element modeling. *Journal of Science and Technology in Civil Engineering (SCTE) - HUCE*, 18(4V):106–121. (in Vietnamese).

[8] ATC-40 (1996). *Seismic evaluation and retrofit of concrete buildings*. Applied Technology Council, Redwood City, California, USA.

[9] FEMA 273 (1997). *NEHRP guidelines for seismic rehabilitation of buildings*. Federal Emergency Management Agency, Washington, D.C., USA.

[10] FEMA 356 (2000). *Prestandard and commentary for seismic rehabilitation of buildings*. Federal Emergency Management Agency, Washington, D.C., USA.

[11] Maaddawy, T. E., Soudki, K., Topper, T. (2005). Analytical model to predict nonlinear flexural behavior of corroded reinforced concrete beams. *ACI Structural Journal*, 102(4):550–559.

[12] Yang, S.-Y., Liu, X.-L., Leng, Y.-B. (2013). Prediction of flexural deformation of a corroded RC beam with a polynomial tension-stiffening model. *Journal of Structural Engineering*, 139(6):940–948.

[13] Ang, B. C., Priestley, M. J. N., Paulay, T. (1989). Seismic shear strength of circular reinforced concrete columns. *ACI Structural Journal*, 86(1):45–59.

[14] Aschheim, M., Moehle, J. P. (1992). *Shear strength and deformability of RC bridge columns subjected to inelastic cyclic displacements*. Report No. UCB/EERC-92/04, Earthquake Engineering Research Center, University of California, Berkeley.

[15] Priestley, M. J. N., Verma, R., Xiao, Y. (1994). Seismic shear strength of reinforced concrete columns. *Journal of Structural Engineering*, 120(8):2310–2329.

[16] Sezen, H., Moehle, J. P. (2004). Shear strength model for lightly reinforced concrete columns. *Journal of Structural Engineering*, 130(11):1692–1703.
[17] ACI 318-19 (2019). *Building code requirements for structural concrete (ACI 318-19) and commentary (ACI 318R-19)*. ACI Committee 318, American Concrete Institute, Farmington Hills, MI.
[18] NZS-3101 (2019). *Code of practice for the design of concrete structures*. Standards Association of New Zealand, Wellington, New Zealand.
[19] Mander, J. B. (1983). Seismic design of bridge piers. PhD thesis, Department of Civil Engineering, University of Canterbury.
[20] Sezen, H., Setzler, E. J. (2008). Reinforcement slip in reinforced concrete columns. *ACI Structural Journal*, 105(3):280–289.
[21] Du, Y. G., Clark, L. A., Chan, A. H. C. (2005). Residual capacity of corroded reinforcing bars. *Magazine of Concrete Research*, 57(3):135–147.
[22] Du, Y. G., Clark, L. A., Chan, A. H. C. (2005). Effect of corrosion on ductility of reinforcing bars. *Magazine of Concrete Research*, 57(7):407–419.
[23] Palsson, R., Mizra, M. S. (2002). Mechanical response of corroded steel reinforcement of abandoned concrete bridge. *ACI Structural Journal*, 99(2):157–162.
[24] Yeh, Y.-K., Mo, Y. L., Yang, C. Y. (2002). Seismic performance of rectangular hollow bridge columns. *Journal of Structural Engineering*, 128(1):60–68.
[25] Dhakal, R. P., Maekawa, K. (2002). Path-dependent cyclic stress–strain relationship of reinforcing bar including buckling. *Engineering Structures*, 24(11):1383–1396.
[26] Kashani, M. M., Crewe, A. J., Alexander, N. A. (2013). Nonlinear stress–strain behaviour of corrosion-damaged reinforcing bars including inelastic buckling. *Engineering Structures*, 48:417–429.
[27] Scribner, C. F. (1986). Reinforcement buckling in reinforced concrete flexure members. *ACI Journal Proceedings*, 83(6):996–973.
[28] Mander, J. B., Priestley, M. J. N., Park, R. (1988). Theoretical stress-strain model for confined concrete. *Journal of Structural Engineering*, 114(8):1804–1826.
[29] Hsu, T. T. C. (1992). *Unified theory of reinforced concrete*. CRC Press, Boca Raton, FL.
[30] Calderone, A. J. (2001). *Behavior of reinforced concrete bridge columns having varying aspect ratios and varying lengths of confinement*. Pacific Earthquake Engineering Research Center, College of Engineering, University of California, Berkeley, CA, USA.
[31] XTRACT 3.0.8 (2007). *Cross-sectional structural analysis of components*.
[32] Paulay, T., Priestley, M. J. N. (1992). *Seismic design of reinforced concrete and masonry building*. John Wiley & Sons, Inc., New York, U.S.A.
[33] Moehle, J. P. (1992). Displacement-based design of RC structures subjected to earthquakes. *Earthquake Spectra*, 8(3):403–428.
[34] Lodhi, M. S., Sezen, H. (2012). Estimation of monotonic behavior of reinforced concrete columns considering shear-flexure-axial load interaction. *Earthquake Engineering & Structural Dynamics*, 41(15): 2159–2175.
[35] Ou, Y.-C., Nguyen, N. D. (2014). Plastic hinge length of corroded reinforced concrete beams. *ACI Structural Journal*, 111(5):1049–1058.